Molecular Crystals and Liquid Crystals

ISSN: 1542-1406 (Print) 1563-5287 (Online) Journal homepage: http://www.tandfonline.com/loi/gmcl20

Nanoporous polyimide film from poly(ethylene glycol-co-imide) using a one-step heat calcination process

Young-Woon Cho, Kyung-Seok Kang, Chanhyuk Jee, Ji-Hyun Kim, Dongju Jang & Pilho Huh

To cite this article: Young-Woon Cho, Kyung-Seok Kang, Chanhyuk Jee, Ji-Hyun Kim, Dongju Jang & Pilho Huh (2016) Nanoporous polyimide film from poly(ethylene glycol-co-imide) using a one-step heat calcination process, Molecular Crystals and Liquid Crystals, 634:1, 73-81, DOI: 10.1080/15421406.2016.1177905

To link to this article: http://dx.doi.org/10.1080/15421406.2016.1177905

Published online: 26 Sep 2016.

MOLECULAR CRYSTALS AND LIQUID CRYSTALS
2016, VOL. 634, 73–81
http://dx.doi.org/10.1080/15421406.2016.1177905

Taylor & Francis
Taylor & Francis Group

Nanoporous polyimide film from poly(ethylene glycol-co-imide) using a one-step heat calcination process

Young-Woon Cho, Kyung-Seok Kang, Chanhyuk Jee, Ji-Hyun Kim, Dongju Jang, and Pilho Huh

Department of Polymer Science and Engineering, Pusan National University, Busan , South Korea

ABSTRACT

Polyamic acid (PAA) made from 3,3, 4,4-biphenyltetracarboxylic dianhydride and 4,4-diaminodiphenyl ether was synthesized and used as the backbone of nanoporous polyimide. Thermally labile polyethylene glycol (PEG) at 10, 20 or 30 wt% was introduced to the end group of PAA. Self-assembled PAA-b-PEG micelle-like nanoparticles could be formed as a result of amphiphilic characteristics of hydrophobic PAA and hydrophilic PEG. Thermal imidization and degradation of spin-coated amphiphilic PAA-b-PEG film were performed sequentially through one-step heat treatment to obtain polyimide film with nanopores. Pore sizes decreased with increasing amount of PEG block and their dielectric constants decreased from 2.71 ± 0.13 to 2.38 ± 0.11.

KEYWORDS

Nanoporous polyimide; poly(ethylene glycol-co-imide); dielectric constant; tensile strength; one-step calcination

Introduction

Porous polyimide (PI) has attracted considerable attention for applications, such as low dielectric insulators, gas separation membranes and light-weight heat insulators. A PI interlayer with a lower dielectric constant is needed to reduce the resistance-capacitance time delays, cross-talk and power dissipation in the large-scale integrated circuits [1,2]. Silicon dioxide with a dielectric constant of 4.0 is expected to be replaced with dielectric materials with ultralow dielectric constants (ultralow-k: $k < 2.0$) in the near future [3]. Moreover, a lighter and more transparent dielectric material is required to develop micro/nano-electronic devices. A range of methods, such as blowing agents [4–6], phase inversion of the cast films [7–10], block copolymer [11], condensing water droplets [12] and colloidal spheres [13], have been reported to be effective tools for preparing porous PI films. A more effective approach for nanoporous PI films is the thermal or chemical degradation of a labile polymer in the PI copolymer [14]. In this approach, poly(propylene oxide) [15,16], poly(propylene glycol) [17,18] and poly(methyl-methacrylate) [19] have been used as the labile block. On the other hand, there are some limitations in that the thermal removal of most labile polymers could overlap closely with the thermal imidization temperature of polyamic acid (PAA) [19,20], and the combination of chemical and thermal imidization is an expensive and lengthy process for mass production.

CONTACT Pilho Huh pilho.huh@pusan.ac.kr Department of Polymer Science and Engineering, Pusan National University, Busan 609-735, South Korea.
Color versions of one or more of the figures in the article can be found online at www.tandfonline.com/gmcl.

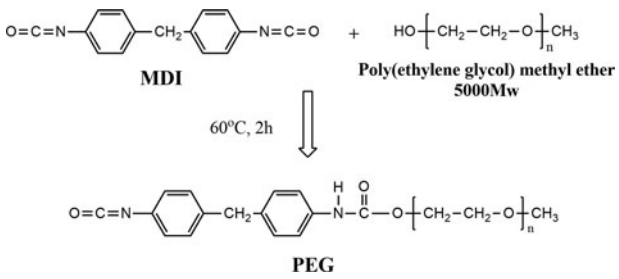

Scheme 1. Synthetic reaction of poly(ethylene glycol) modified with diisocyanate.

To overcome these drawbacks, a nanoporous PI film should be composed of a thermally stable imide component and a thermally labile polymer block. Thermal treatment above the imidization temperature causes the degradation of only the labile blocks, leaving the nanoporous polyimide films.

In this study, a one-step calcination process to prepare a PI film with uniform nanopores and a low dielectric value was demonstrated. Polyethylene glycol (PEG) with a thermal degradation temperature above 250°C was cooperated successfully with the end group of PAA. Imidization and nanopore formation of the spin-coated PAA-PEG films were carried out easily using a one-step heat treatment, ranging from 110°C to 300°C. The imidization of PAA occurred at approximately 210°C, whereas the thermal degradation of PEG blocks in the PAA-*b*-PEG began at approximately 280°C. The thermal stability, dielectric constants and mechanical properties of the resulting nanoporous PI films containing various PEG contents were compared with those of a bulk PI film.

Experimental

Materials

3,3′,4,4′-Biphenyltetracarboxylic dianhydride (BPDA) and poly(ethylene glycol) methyl ether (M_n = 5000) were purchased from Aldrich Chemical Co and used as received. 4,4′-Diaminodiphenyl ether (ODA) (Wako Chemical Co.), N,N-dimethyl-acetamide (DMAc) (TCI Chemical Co.) and 4,4'-diphenylmethane diisocyanate (MDI) (Juncei Chemical Co.) were used as received. All materials were used without further purification.

Synthesis of poly(ethylene glycol) (PEG)

Scheme 1 presents the modified procedure of thermally labile PEG. In a 250 ml four-necked round-bottomed flack fitted with a mechanical stirrer, a mixture of poly(ethylene glycol) methyl ether (M_n = 5000, 20.0 g, 4 mmol) and 4,4'-diphenylmethane diisocyanate (MDI) (1.0 g, 4 mmol) was stirred vigorously at 60°C for 2 h under a nitrogen atmosphere.

Synthesis of poly(ethylene glycol-co-imide)

Scheme 2 shows a schematic diagram of the procedure to synthesize PAA-*b*-PEG. BPDA (1.147 g, 3.9 mmol) and DMAc (10 ml) were placed in a 250 ml four-necked flask, and the solution was stirred vigorously at 0°C for 30 min under a nitrogen atmosphere. ODA (0.801 g, 4.0 mmol) was then added. The mixture was stirred vigorously at 0°C for 1 h and continually at room temperature for 6 h. Various amounts of PEG (10, 20 and 30 wt.%) were added

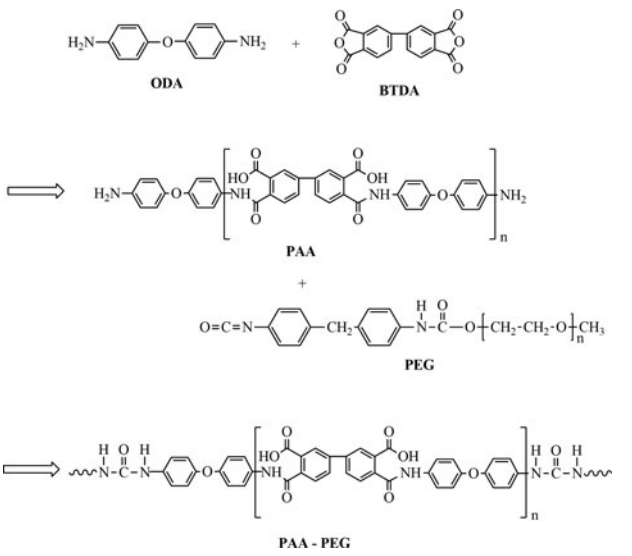

Scheme 2. A schematic procedure to synthesize PAA-*b*-PEG copolymer via chemical combination of polyamic acid and modified PEG.

to the PAA solution and the mixture was stirred further at room temperature for 24 h. The synthesized solution was stored in a refrigerator prior to use.

Preparation of porous polyimide film

PAA-*b*-PEG was spin-coated on a glass substrate at a spin speed of 500 rpm. The residual solvents of the spin-coated PAA-*b*-PEG films were evaporated in a vacuum oven at 50°C for 2 h. The dried PAA-*b*-PEG films were imidized further by sequential heating at 110, 150, 180 and 210°C for 30 min in a vacuum oven. Nanopores were formed by the thermal degradation of PEG blocks at 300°C for 3 h in a vacuum oven.

Measurements

Fourier transform infrared (FT-IR) spectroscopy was performed using a Cary 600 Series FT-IR spectrometer from Agilent Technologies. The nuclear magnetic resonance (NMR) spectra were obtained on a Unity Inova 500 spectrometer (Varian, Palo Alto, CA, USA) operating at 500 MHz for ^{1}H at 25°C. The morphology of nanoporous films was analyzed by a field emission scanning electron microscopy (FE-SEM, Zeiss SUPRA 40 VP). Dielectric measurement of the PI film was performed using an impedance analyzer HP 4380A at room temperature air-atmosphere. Au electrode with about 50 nm thickness was sputtered on both side film surfaces to ensure a good electronic contact. The dielectric constant of the individual sample was determined under applying a frequency of 1 MHz. Thermal analysis was conducted in air on a Perkin-Elmer STA 6000 with a heating rate of 10°C min^{-1} over temperature range, 30°C–900°C. Spin-coating was carried out using an ACE-200 spin coater from Dongah Tech., Korea and the film thickness was measured using a Dektak3 surface profiler from Vecco Instrument Inc. The tensile properties of the PI films with the nanopores were evaluated using a universal testing machine (Lloyd LRX) at a crosshead speed of 5 mm min^{-1} using the specimens prepared according to the ASTM D-1822.

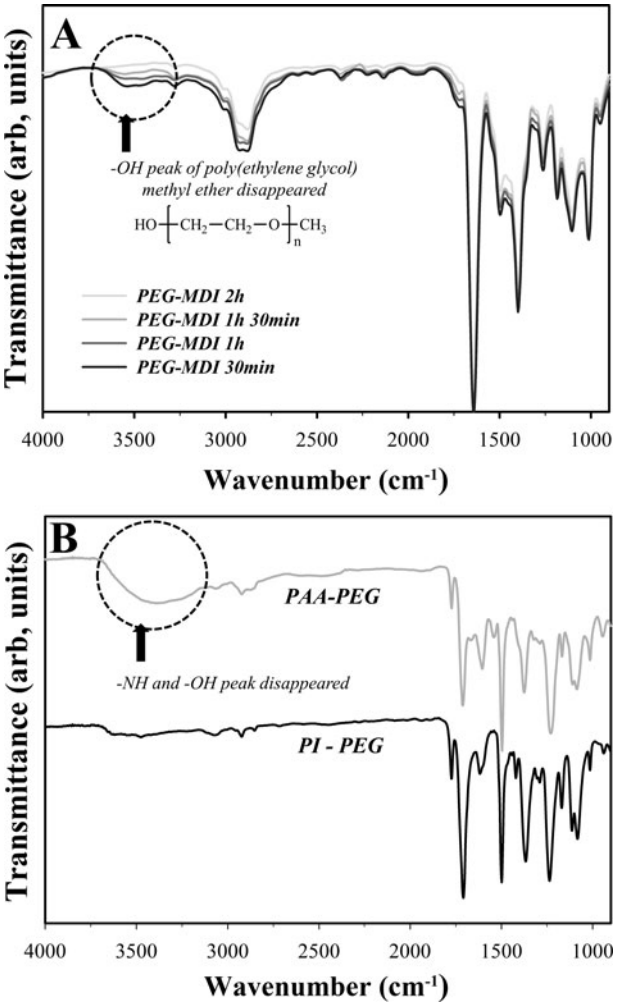

Figure 1. FT-IR spectra of (a) PEG-MDI at in situ synthesizing and (b) PAA-*b*-PEG before imidazation and PI-*b*-PEG after imidazation.

Results and discussion

FT-IR and NMR analysis

Figure 1 shows the FT-IR spectra to characterize the chemical structure of PEG-MDI, PAA-*b*-PEG and PI-*b*-PEG. The chemical combination of PEG and 4,4'-diphenylmethane diisocyanate (MDI) was confirmed by comparing the FT-IR spectrum of bulk PEG. The OH peak of the PEG was decreased to approximately 3200–3600 cm^{-1}, as shown in Fig. 1(a). The specific NH and OH peaks of PAA-*b*-PEG at approximately 3200–3600 cm^{-1} disappeared with thermally imidization ranging from 110°C to 210°C, as evidenced from Fig. 1(b).

Figure 2 shows the detailed characteristic peaks of PAA-*b*-PEG, PI-*b*-PEG and nanoporous PI. Strong peak around 1700 cm^{-1} could be assigned to the carbonyl stretch of urethane bond. The presence of C=O peak at 1700 cm^{-1} indicated that hydrogen bonding was formed. A characteristic peak of PI as C=O symmetric stretching and the carbonyl peak of urethane group could be overlapped at around 1700 cm^{-1}. As a result, absorption band around

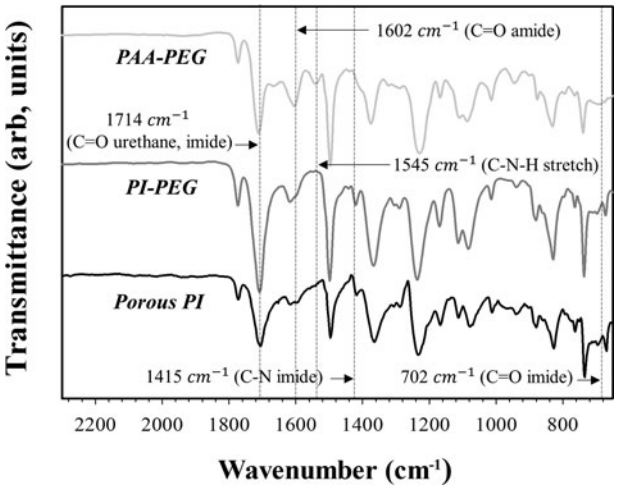

Figure 2. FT-IR spectra of PAA-*b*-PEG before imidazation and PI-*b*- PEG after imidazation and nanoporous PI.

1700 cm^{-1} could not provide any difference between PAA-PEG and PI-PEG as shown in Fig. 2. The presence and absence of the C–N–H stretching at 1545 cm^{-1} before/after thermal degradation of PEG blocks indicated the imidization of the PI-PEG film and the formation of nanoporous PI film. The results suggest that PAA-*b*-PEG had been converted completely to PI-*b*-PEG through thermal imidization.

Figure 3 shows the ^{1}H NMR spectra of PI-*b*-PEG films prior to calcination at 300°C. The characteristic proton peak at 7.9–8.5 ppm indicated the presence of a biphenyl structure. The signals at 6.5–7.8 ppm were assigned to the diamine segment and the signals at 6 ppm were attributed to the urea group. The methyl proton peaks of the PEG blocks were also observed at 3.2 ppm. Some traces of residual solvent were detected in the range, 2.9–1.9 ppm.

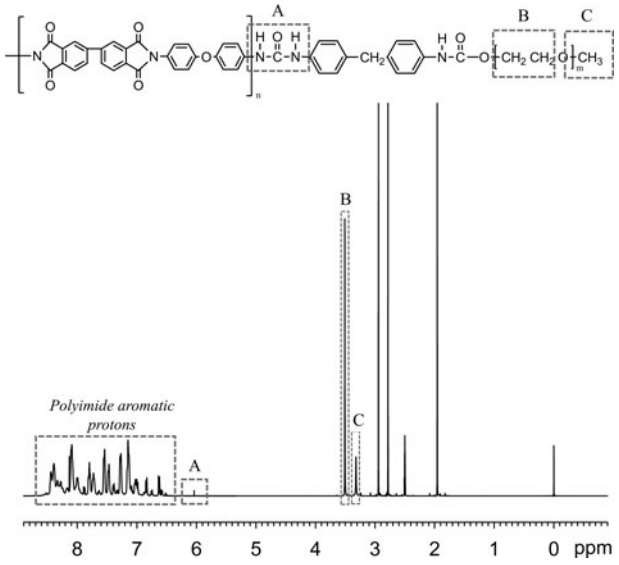

Figure 3. ^{1}H NMR spectrum of PI-*b*-PEG imidized ranging from 110°C to 210°C.

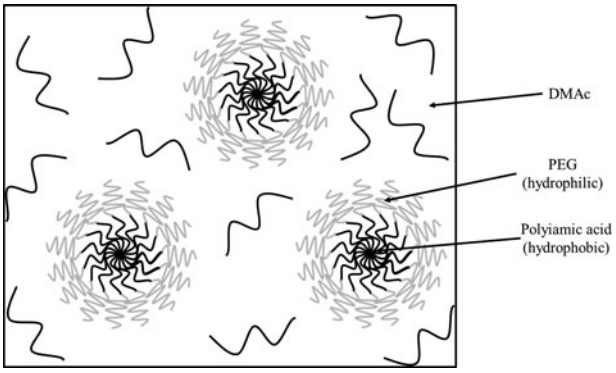

Scheme 3. Micelle-structure of amphiphilic PAA-*b*-PEG.

Scanning electron microscopy (SEM)

As illustrated in Scheme 3, the hydrophilic PEG domains can form micellar corona that may provide a protective surface between the hydrophobic PAA micellar core and the externally hydrophilic DMAc solvent.

The existence of nanopores on the calcined PI films was confirmed by FE-SEM, as shown in Fig. 4. PI films with uniform nanopores were formed successfully by thermal imidization and degradation by a one-step calcination process of amphiphilic PAA-*b*-PEG copolymer, ranging from 110°C to 300°C. The resulting pores were almost spherical in shape with a homogenous distribution without any interconnections in the overall area of the PI films. The mean pore size of the PI film containing 10 wt.% PEG was approximately 2 μm in diameter and a 20 wt.% block of PEG provided an average pore size of 800 nm. The pore size varied considerably with the PEG contents and the average diameter of 30 wt.% PEG blocks was approximately 400 nm. This indicates that the amount of PEG blocks in PAA-*b*-PEG was a key factor in controlling the pore size. The formation of a much smaller pore size by the increase in PEG content in PAA-*b*-PEG may explain the characteristics of the amphiphilic copolymer micelles, i.e., a lower

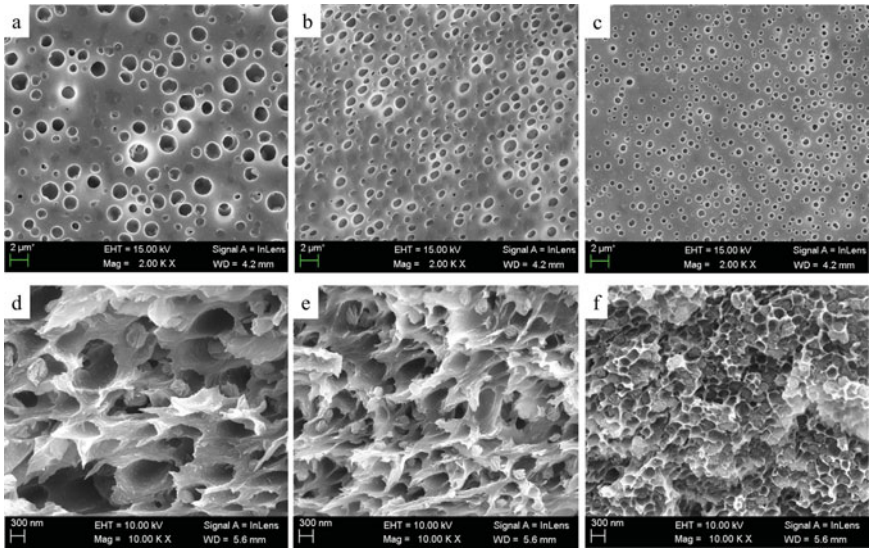

Figure 4. (a), (b), (c) Surface and (d), (e), (f) cross-sectional SEM images of porous PI films formed by calcining PEG blocks of (a), (d) 10 wt.%, (b), (e) 20 wt.% and (c), (f) 30 wt.%.

Table 1. Mechanical properties of porous PI films with different PEG blocks of 10, 20, and 30 wt. %.

PEG contents	Films thikness (μm)	Max. stress (MPa)	Max. elongation(%)	T5[a](°C)	T10[b](°C)	Char yield[c] (%)
Bulk PI	4–5	184 ± 4	8.3 ± 0.3	575	596	66.2
10 wt.%	4–5	181 ± 5	8.1 ± 0.3	576	601	62.2
20 wt.%	4–5	155 ± 4	6.1 ± 0.3	574	594	60.1
30 wt.%	4–5	108 ± 3	5.3 ± 0.3	572	594	59.5
PEG	—	—	—	310	332	0.8

[a]Temperature at which 5% weight loss was recorded by TGA.
[b]Temperature at which 10% weight loss was recorded by TGA.
[c]Residual weight retention when heated to 800°C in nitrogen.

hydrophobic component results in smaller micelles]21,22]. In giving a fixed amount of PAA-*b*-PEG copolymer, the decrease in the PAA to PEG ratio in polymer composition may explain the decrease in the pore size of the PI film. Interestingly, a number of particles were observed within the pores of a cross-section of the nanoporous PI films (Figs. 4(d) and (e)). These particles may have formed from the amphiphilic copolymer micelles. The outside (PEG segment) of the amphiphilic copolymer micelles will decompose, whereas the inside (PI segment) will not.

Mechanical properties

The mechanical properties of the PI films containing nanopores were evaluated using a stress–strain (S-S) test as a function of the PEG content. Table 1 lists the mechanical properties of the nanoporous PI films at approximately 4.5 μm. Nanoporous PI films with low PEG contents showed a larger elongation at break and were more flexible. When the content of PEG blocks was increased from 10 to 30 wt.%, the maximum stress decreased and the average Young's modulus and ductility were relatively unchanged, as shown in Table 1. This suggests that mechanical behavior of nanoporous PI films depends on the PEG content. The reduced modulus can be explained by the film density [23] and grain boundary compliance]24,25]. As the amount of PEG blocks increases, the grain boundaries may occupy a significant part of the film [26], and may become elastically softer than the grain interior, resulting in a reduced modulus]27,28].

Dielectric constants and thermal analysis

Figure 5 and Table 2 present the dielectric constants of the nanoporous PI films as a function of the PEG content. The dielectric constant decreased with increasing PEG content. The PI film chemically embedded with 20 wt.% PEG blocks had a relatively low dielectric constant of 2.60 ± 0.09 compared to that of the bulk PI film. This was attributed to the incorporation of pores into the PI by the thermal degradation of labile PEG blocks. The presence of nanopores in a PI film could allow an increase in free volume, which has a dielectric constant of one. The PI film with 30 wt.% PEG showed the lowest value of 2.38 ± 0.11. The nanoporous PI film containing 10 wt.% PEG had a relatively high dielectric constant of 2.71 ± 0.13.

Figure 6 shows the thermogravimetric analysis (TGA) curves to examine the thermal properties of PI-*b*-PEG films containing 10, 20 and 30 wt.% PEG blocks in air. The PAA-*b*-PEG was converted to PI-*b*-PEG due to the imidization of PAA in the range, 110°C–210°C. A comparison of the decomposition profile of the bulk PI and PI-*b*-PEG with different PEG revealed the bulk PI film to undergo one-step decomposition, whereas the nanoporous PI films

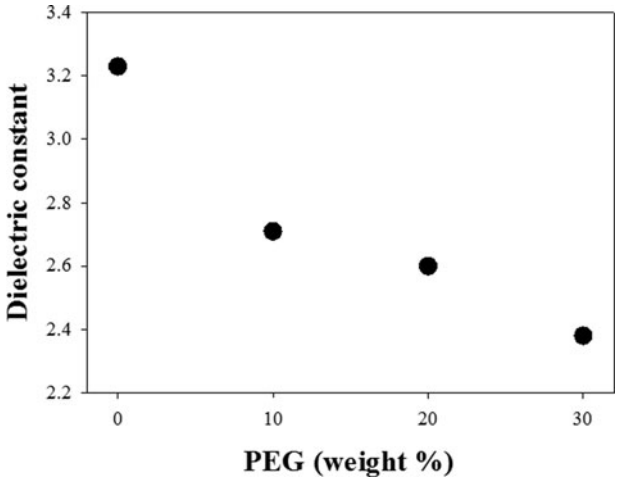

Figure 5. Dielectric constants of bulk PI and porous PI films with various weight percentages of PEG block.

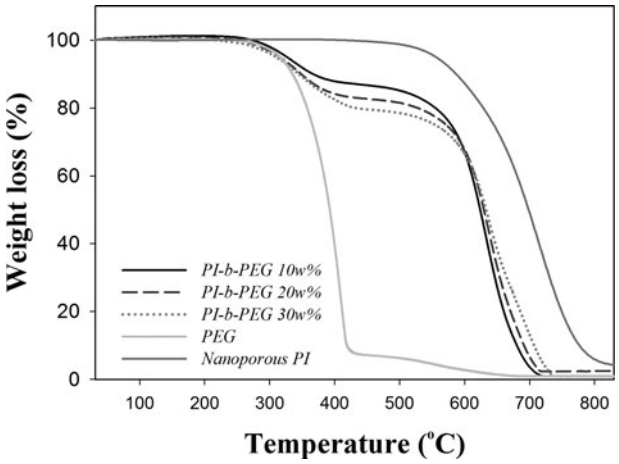

Figure 6. TGA thermograms of PEG and porous PI films prepared at different PEG contents of 10, 20 and 30 wt.% by one-step calcination process in the air.

underwent two-step decomposition. The first decomposition of the PEG blocks occurred at around 290°C. The second decomposition of imide component began at approximately 570°C. The results suggest that heat treatment of the PI-*b*-PEG film, ranging from 280°C to 570°C, could lead to the thermal degradation of PEG blocks only, leaving nanoporous polyimide films. The increase in total weight loss was attributed to an increase in the PEG content of the PI-*b*-PEG film. Thermal degradation region of PEG blocks was not observed in nanoporous PI. As a result, Fig. 6 shows that decomposition temperature of nanoporous PI corresponds to that of PI-b-PEG.

Table 2. Dielectric constants of bulk PI and porous PI films formed by the calcination of various PEG contents.

PEG contents	Bulk PI	10 wt.%	20 wt.%	30 wt.%
Dielectric constant	3.23 ± 0.28	2.71 ± 0.13	2.60 ± 0.09	2.38 ± 0.11

Conclusions

Nanoporous PI films with a spherical shape and homogenous distribution were prepared using PEG as a thermally labile block. The formed pore size could be controlled by changing the PEG contents. The pore size decreased with increasing PEG content due to the characteristics of amphiphilic PAA-*b*-PEG copolymer micelles. The decrease in the PEG blocks of the PI film tended to show a low elastic modulus and more flexibility due to the relatively low pore density. The tensile strengths of the nanoporous PI films decreased due to pore density and grain boundary; however, their tensile strain increased accordingly. The dielectric constant of the nanoporous PI films could be controlled by varying the amount of PEG block. The nanopore size decreased with decreasing PEG content. The pore size could also be controlled by the amount of the labile block embedded chemically in PAA-PEG.

Funding

This work was supported by the Brain Korea 21 Project funded by the Ministry of Education, Science and Technology, Korea and Pusan National University Research Grant, 2014.

References

[1] Martin, S. J., Godschalx, J. P., Mills, M. E., Shaffer, E. O., & Townsend, P. H. (2000). *Adv. Mater.*, *12*, 1769–1778.
[2] Maier, G. (2001). *Prog. Polym. Sci.*, *26*, 3–65.
[3] Volksen, W., Miller, R. D., & Dubois, G. (2009). *Chem. Rev.*, *110*, 56–110.
[4] Hoenig, S. M., & Lancaster, G. M. (1985). U.S. Patent Number 4,535,100.
[5] Hoki, T., & Matsuki, Y. (1986). U.S. Patent Number 4,629,745.
[6] Smearing, R. W., & Floryan, D. E. (1985). U.S. Patent Number 4,543,368.
[7] Yanagishita, H., Kitamoto, D., & Nakane, T. (1995). *High Perform. Polym.*, *7*, 275–281.
[8] Kawakami, H., & Nagaoka, S. (1995). *ASAIO J.*, *41*, M379–M383.
[9] Echigo, Y., Iwaya, Y., Saito, M., & Tomioka, I. (1995). *Macromolecules*, *28*, 6684–6686.
[10] Hatori, H., Yamada, Y., & Shiraishi, M. J. (1995). *Appl. Polym. Sci.*, *57*, 871–876.
[11] Li, X. et al., (2010). *Mater. Chem.*, *20*, 4333–4339.
[12] Li, L. et al., (2009). *Chem. Mater.*, *21*, 4977–4983.
[13] You, B. et al., (2008). *Macromolecules*, *41*, 6624–6626.
[14] Hedrick, J. L. et al., (1999). *Adv. Polym. Sci.*, *141*, 1–43.
[15] Carter, K. R., DiPietro, R. A., Sanchez, M. I., & Swanson, S. A. (2001). *Chem. Mater.*, *13*, 213–221.
[16] Chung, C. M., Lee, J. H., Cho, S. Y., Kim, J. G., & Moon, S. Y. (2006). *J. Appl. Polym. Sci.*, *101*, 532–538.
[17] Hedrick, J. L., Charlier, Y., DiPietro, R., Jayaraman, S., & McGrath, J. E. (1996). *J. Polym. Sci. Part A Polym. Chem.*, *34*, 2867–2877.
[18] Choi, J. Y., Takayama, T., Yu, H. C., Chung, C. M., & Kudo, K. (2012). *Polymer*, *53*, 1328–1338.
[19] Miyata, S., Yoshida, K., Shirokura, H., Kashio, M., & Nagai, K. (2009). *Polym. Int.*, *58*, 1148–1159.
[20] Fu, G. D., Zong, B. Y., Kang, E. T., & Neoh, K. G. (2004). *Ind. Eng. Chem. Res.*, *43*, 6723–6730.
[21] Tuzar, Z., & Kratochvil, P. (1976). *Adv. Colloid Interface Sci.*, *6*, 201–232.
[22] Hu, Y. et al., (2003). *Biomaterials*, *24*, 2395–2404.
[23] Sanders, P. G., Eastman, J. A., & Weertman, J. R. (1997). *Acta Mater.*, *45*, 4019–4025.
[24] Huang, H., & Spaepen, F. (2000). *Acta Mater.*, *48*, 3261–3269.
[25] Shen, T., Koch, C., Tsui, T., & Pharr, G. J. (1995). *Mater. Res.*, *10*, 2892–2896.
[26] Siegel, R. W., & Thomas, G. J. (1992). *Ultramicroscopy*, *40*, 376–384.
[27] Schiøtz, J., Di Tolla, F. D., & Jacobsen, K. W. (1977). *System*, *214*, 300–315.
[28] Haque, M. A., & Saif, M.T.A. (2004). *Proc. Natl. Acad. Sci. USA*, *101*, 6335–6340.